Supplementary Materials for

Bactericidal Mechanisms Revealed for Rapid Water Disinfection by Superabsorbent Cryogels Decorated with Silver Nanoparticles

Siew-Leng Loo[†,‡], William B. Krantz[†,§], Anthony G. Fane[†,‡], Yiben Gao[†,‡], Teik-Thye Lim[*,†,‡], Xiao Hu[*,†,‖]

[†]Singapore Membrane Technology Centre, Nanyang Environment and Water Research Institute, Nanyang Technological University, 1 Cleantech Loop, CleanTech One, #05-05, Singapore 637141, Singapore.

[‡]School of Civil and Environmental Engineering, Nanyang Technological University, Block N1, 50 Nanyang Avenue, Singapore 639798, Singapore.

[§]Department of Chemical and Biological Engineering, University of Colorado, Boulder, Colorado 80309-0424, USA.

[‖]School of Materials Science and Engineering, Nanyang Technological University, Singapore 639798, Singapore.

*Corresponding author: Tel.: +65 67906933; Fax: +65 67910676; Email: cttlim@ntu.edu.sg

[*]Corresponding author at: School of Materials Science and Engineering, Nanyang Technological University, Singapore 639798, Singapore. Tel: +65 67904610; Fax: +65 68909081; Email: ASXHU@ntu.edu.sg

This file contains a total of 18 pages of supporting materials for the article that includes:

Additional method description
Fig. S1 to S15

Additional method description

Preparation of cryogel nanocomposites

PSA cryogels were prepared by copolymerizing sodium acrylate (SA) monomer and *N,N'*-methylenebis(acrylamide) (MBA) crosslinker at –20 ºC with ammonium persulfate (1.75 mM) and *N,N,N',N'*-tetramethylethylenediamine (0.125% v/v) as the initiator and activator, respectively; the total monomer concentration and crosslinker ratio used was 8% (SA + MBA) and 0.05 (mol MBA/mol SA), respectively. After 24 h, the PSA cryogels were sliced into the desired size followed by thorough washing in MilliQ water and dehydration in *t*-butanol. The cryogels then were placed in a freeze-dryer (Alpha 1-4LD, –45 °C). PSA/AgNP cryogels of various Ag content were prepared by immersing the dried PSA cryogels in Ag^+ solutions of varying concentrations (0.025 mM to 10 mM) at a ratio of 1:250 (g of gel/mL of solution) for 24 h in the dark. The resultant cryogels were then reduced in $NaBH_4$ solution (10:1 molar ratio of $NaBH_4$ to Ag^+) having the same volume as the precursor Ag^+ solution. Note that the $NaBH_4$ reduction step is omitted for the PSA/Ag^+ cryogel synthesis. After equilibration of the cryogels in Ag^+, precautionary steps were taken to avoid light exposure to minimize photo-reduction of Ag^+ to Ag^0 in the cryogels. The resultant cryogels were thoroughly washed by immersion in MilliQ water and vacuum filtration, followed by freeze-drying. The as-synthesized PSA/AgNP cryogel nanocomposites were denoted as AgNC-x, where x represents the Ag content (mg/g) in the cryogel.

1.2 Quantification of pore architecture parameters of the PSA cryogels

Thresholded 2D and 3D images were analyzed using ImageJ software. Two-dimensional images were used for the determination of the mean pore size of the PSA cryogels. Pore interconnectivity, porosity, surface area, and strut thickness were quantified using the 3D

images from reconstruction of the optical slices obtained from X-ray micro-CT. To determine the pore interconnectivity, the thresholded 3D image was inverted to measure the volume of all pore spaces using the Object Counter3D plugin.[1] The same (inverted) thresholded image then was "purified" to contain only the interconnected pores using the command, "purify" in BoneJ plugin.[2] The volume of this region-grown mask that represents the volume of the interconnected pores also was determined. Pore interconnectivity was computed by taking the ratio of the volume of interconnected pores to that of the total pore volume.[3,4] The porosity was determined by subtracting the volume fraction (of the cryogel) from 1.[3] The volume fraction was determined using BoneJ.[2] The surface area of the pores were obtained using the "Object Counter3D" plugin.[1] The value obtained for the pore surface area was normalized with respect to the total volume of cryogel used for the image analysis.[5] The strut thickness was determined by measuring the thickness of the trabeculae (pore walls) using BoneJ.[2]

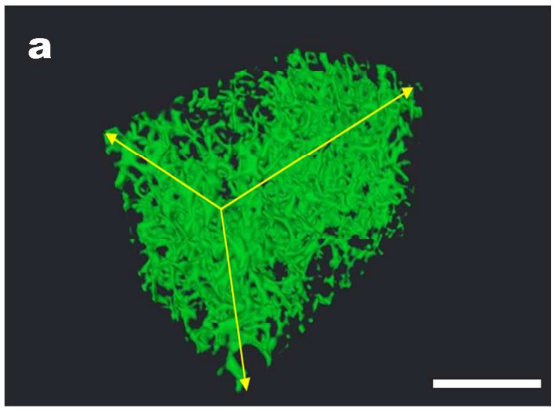

b

Pore architecture parameters	
Interconnectivity (%)	99.97
Porosity (%)	68.3 ± 1.5
Surface area ($\mu m^2/\mu m^3$)	0.035 ± 0.002
Pore size (μm)	16.5 ± 2.7
Strut thickness (μm)	2.1 ± 0.5

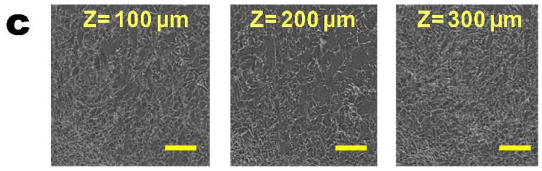

Fig. S1 X-ray microcomputed tomographic characterization of PSA a cryogel. (a) 3D reconstructed image of the cryogel. (b) Summary of quantitative pore parameters of PSA cryogels. (c) X-ray microtomography images of PSA cryogels taken at different sample depths (Z). Note: all the scale bars represent 50 μm length.

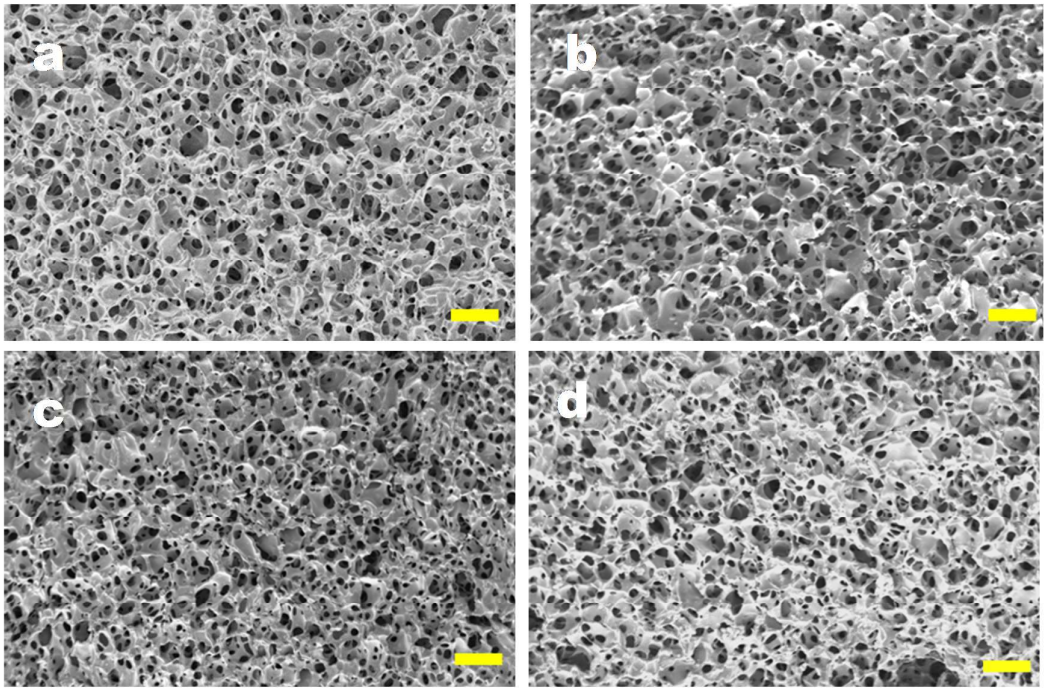

Fig. S2 Morphology of PSA/AgNP cryogels (a) before (b) after 10 cycles, (c) after 100 cycles, and (d) after 1000 cycles of compression; the scale bar denotes 100 μm.

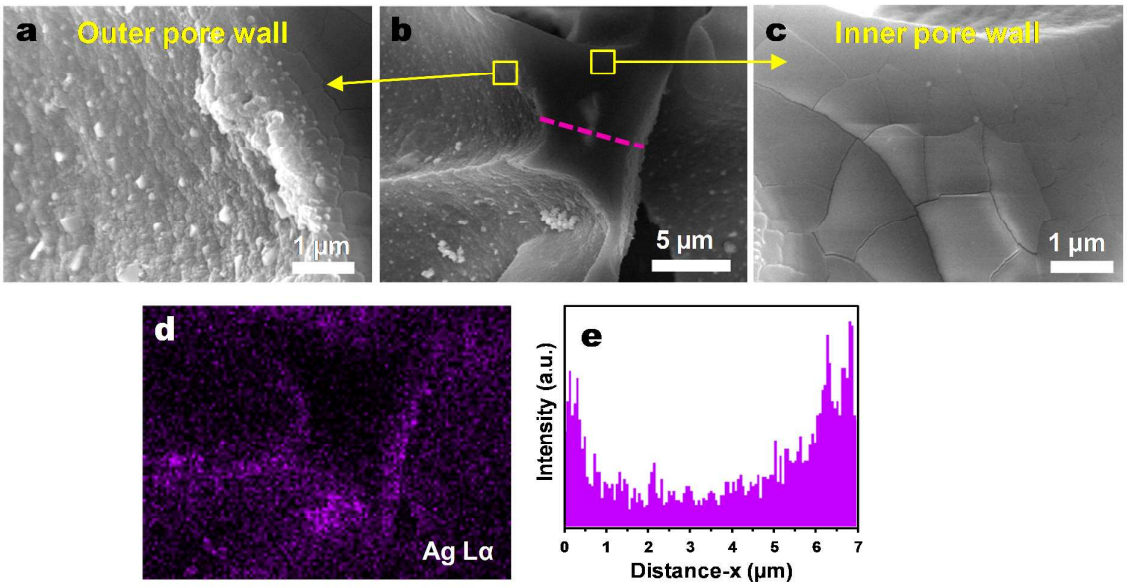

Fig. S3 Distribution of AgNPs in PSA/AgNP cryogel matrix. (b) FESEM image of the cross-section of a pore strut that reveals the morphology of its inner wall, which is the star-shaped middle region. High-magnification FESEM images of the (a) outer and (c) inner pore walls. (d) Ag elemental mapping corresponding to the FESEM image shown in (b). (e) EDX linescan showing the distribution of Ag along the cross-section of the pore strut as indicated by the purple line in (b).

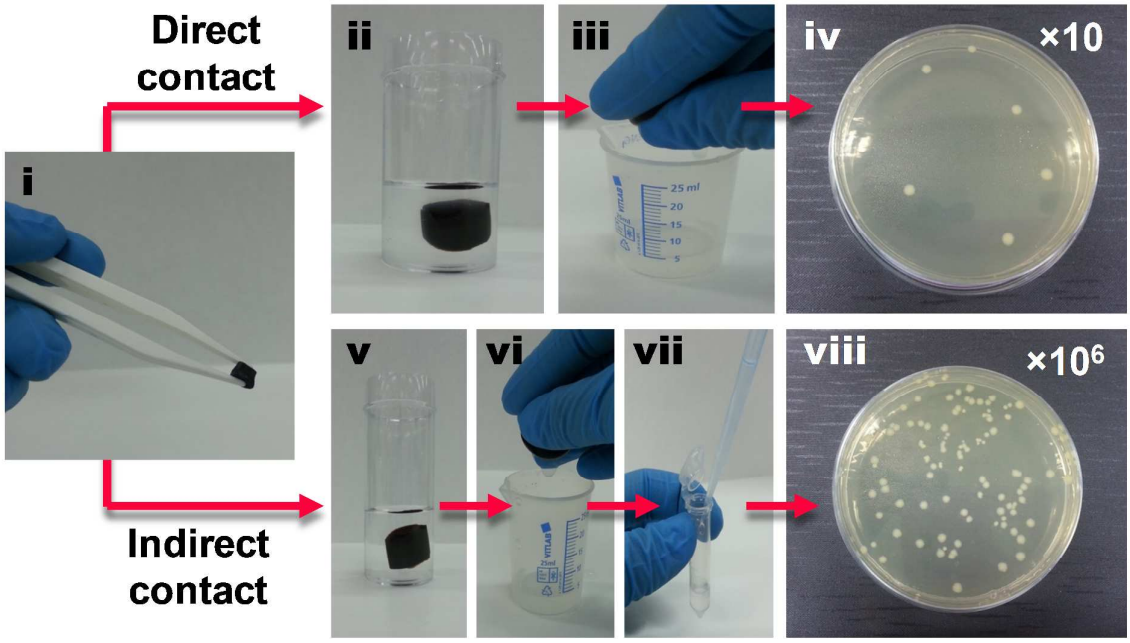

Fig. S4 Summary of the procedure used to compare the disinfection efficacies of the cryogels via direct and indirect contact. For direct contact, the PSA/AgNP cryogel was allowed to swell in a bacterial suspension (for 5 min) after which the absorbed water was squeezed out and directly plated (i-iv). For indirect contact, the PSA/AgNP cryogel first was allowed to swell in PBS for 5 min (v). Then 1 mL of the PBS squeezed from the gel was added to a bacterial pellet and thoroughly mixed for another 5 min before it was plated (vi-vii).

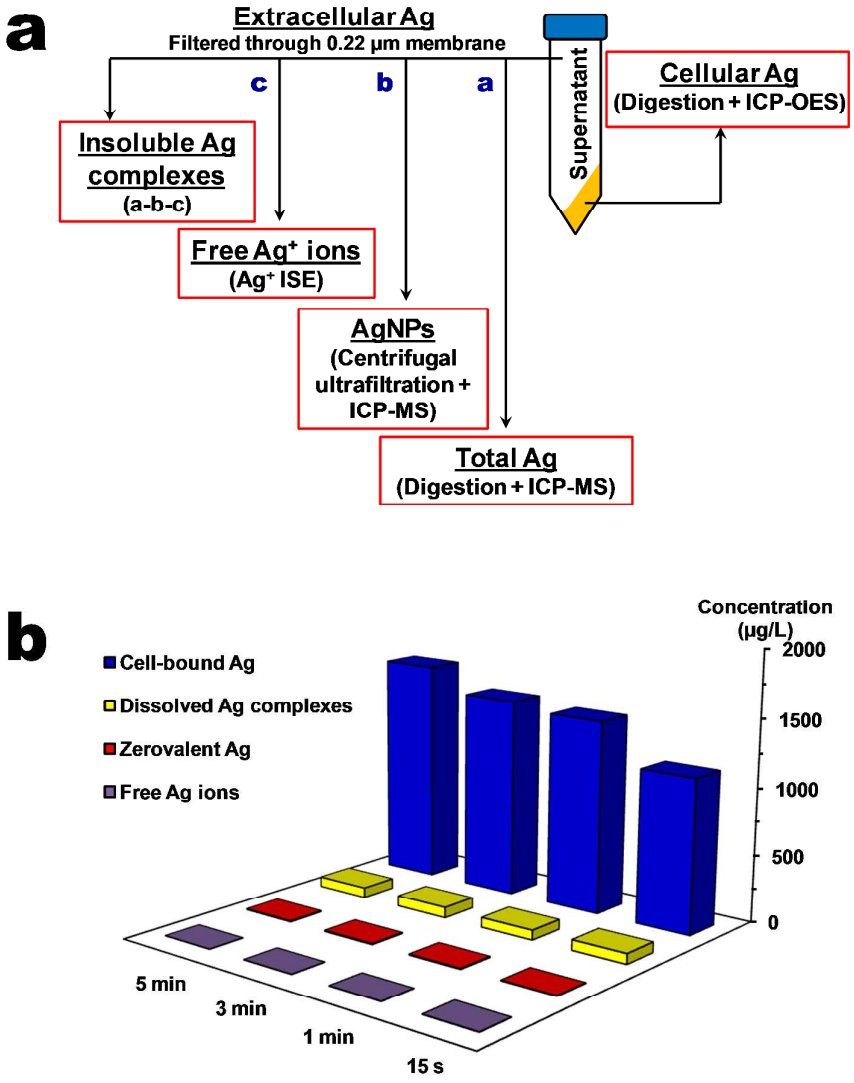

Fig. S5 (a) Schematic detailing the procedure employed for the Ag speciation study. (b) Distribution of Ag species of bacterial suspension exposed to PSA/AgNP cryogels at various contact times.

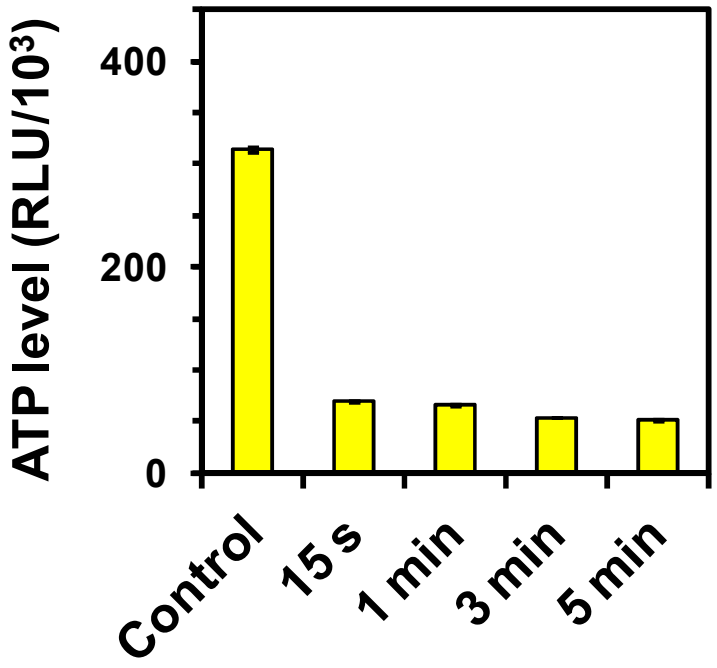

Fig. S6 ATP content in cells exposed to AgNC-170 for various contact times; note: RLU denotes the relative luminescence unit.

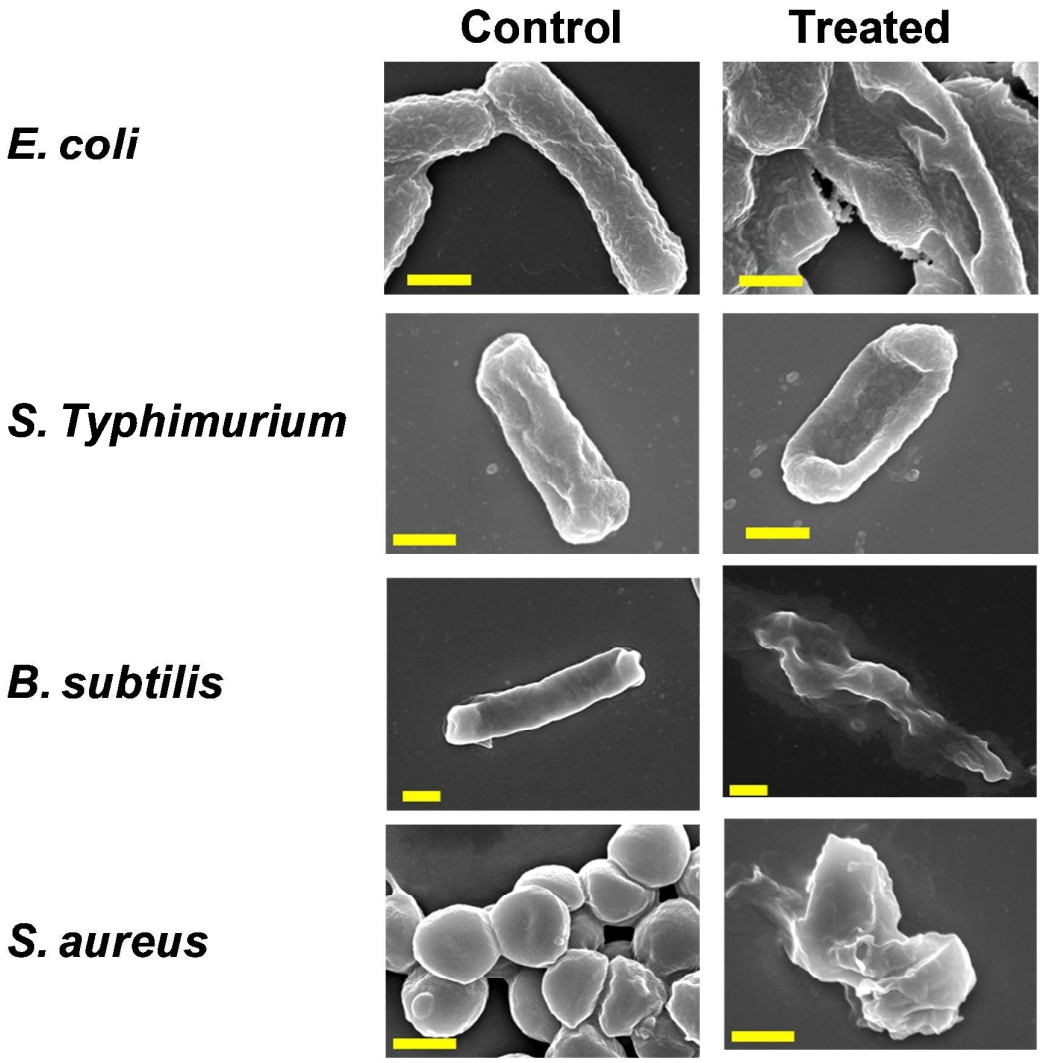

Fig. S7 FESEM images of various types of bacteria before and after exposure to PSA/AgNP cryogels for a 5-min contact time; the scale bars denote 0.5 µm length.

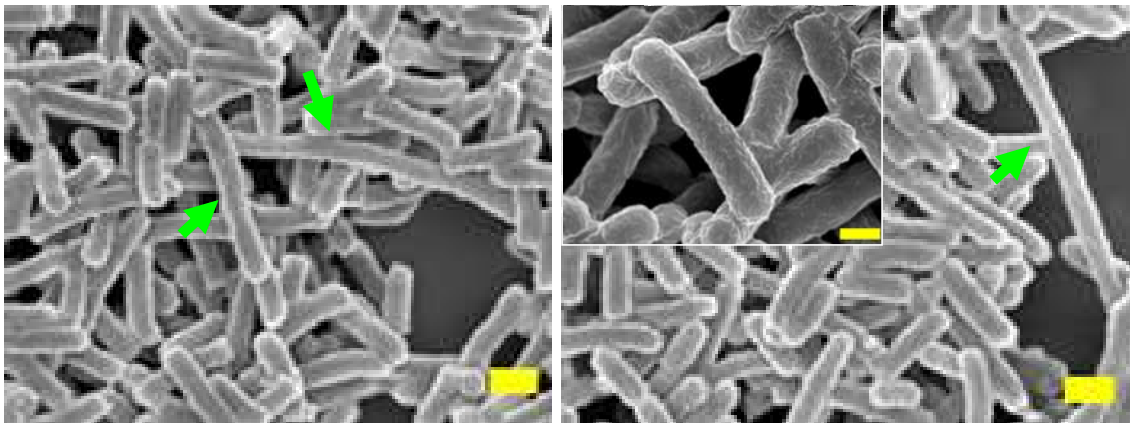

Fig. S8 FESEM images of *E. coli* cells after being exposed to PSA/Ag^{+} cryogels for 5 min. Note that the green arrows are pointing to elongated stressed cells. The scale bars represent 0.5 μm.

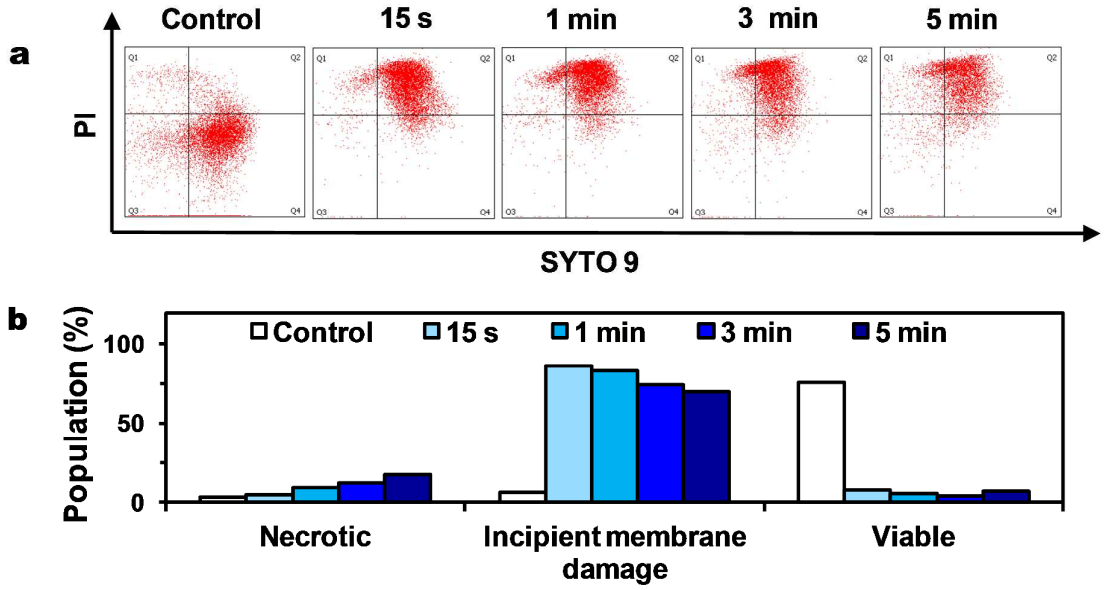

Fig. S9 (a) Cytograms depicting the red versus green fluorescence intensities of *E. coli* cells exposed to PSA/AgNP cryogels as a function of contact time. (b) Variation of the population of gated cells as a function of contact time; necrotic (Q1); incipient membrane damage (Q2); viable cells (Q4); background noise (Q4). A total of 10,000 cells were analyzed for each sample. The four distinct quadrants of the dot plot were determined based on the gating of green (horizontal gate) and red controls (vertical gate).

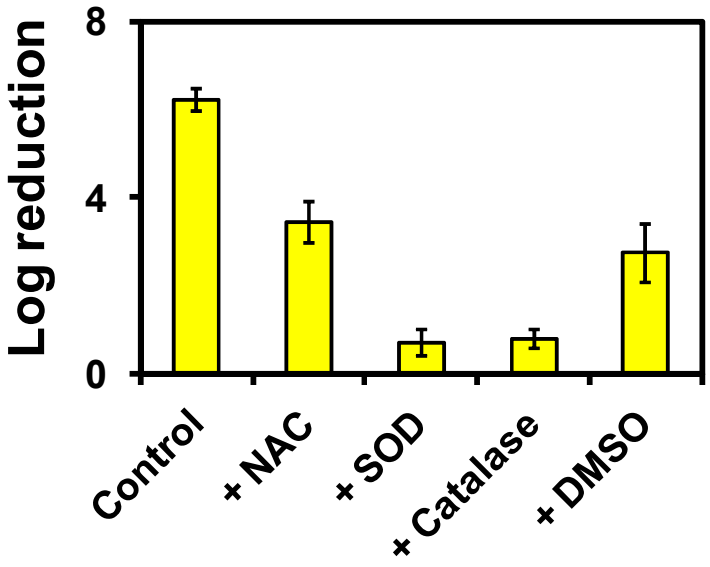

Fig. S10 Antibacterial activity of PSA/AgNP cryogels towards *E. coli* in the presence of different ROS scavengers. Note that the scavengers were added at different concentrations. Hence, the extent of reduction in the antibacterial activities is not proportional to the contribution of the specific ROS quenched by the scavenger. Note: NAC increases the production of glutathione, which is an antioxidant; SOD catalyzes dismutation of $\cdot O_2^-$ to H_2O_2; catalase scavenges H_2O_2; DMSO scavenges $\cdot OH$.

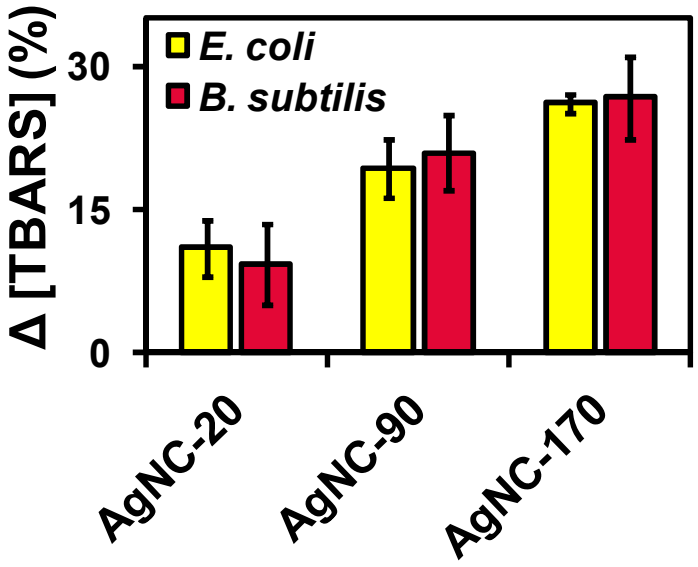

Fig. S11 Comparison of TBARS (thiobarbituric acid reactive substances) level in healthy bacterial cells versus those exposed to PSA/AgNP cryogels.

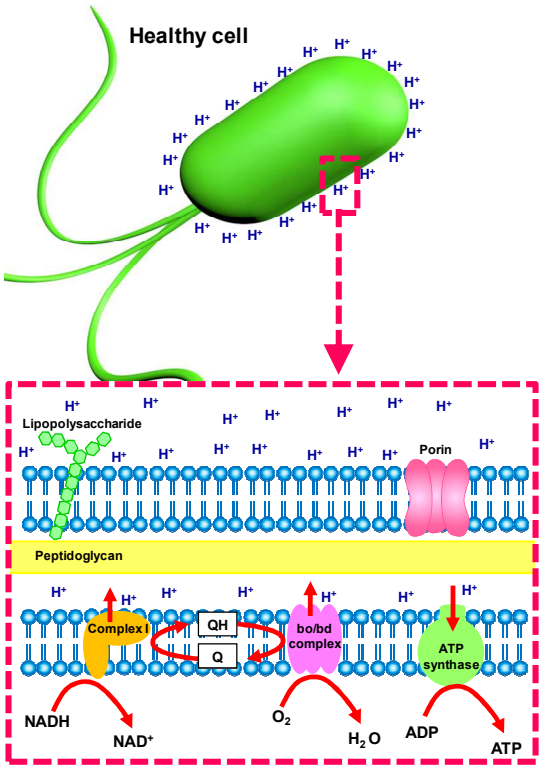

Fig. S12 Illustration depicting the metabolic processes occurring at the bacterial cytoplasmic membrane that serves as the oxidative phosphorylation site. In healthy cells, protons are continuously pumped out of the cells (via coupling proteins) using the energy generated by the transfer of electrons from electron donors (NADH) to electron acceptors (O_2) via redox reactions. This creates an electrochemical gradient for chemiosmosis of a proton back into the cell that generates ATP via phosphorylation of ADP.

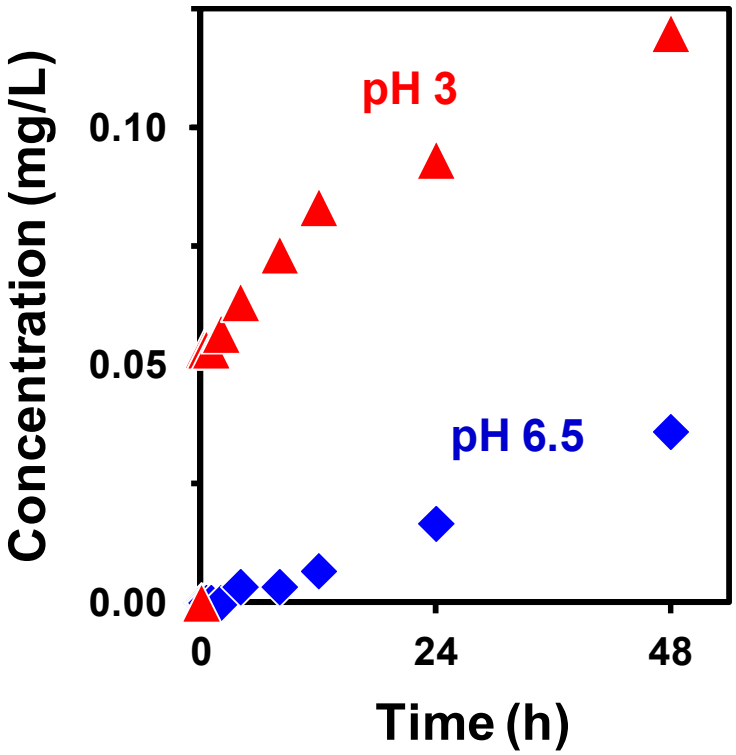

Fig. S13 Effect of pH on the time course for abiotic Ag leaching of PSA/AgNP cryogels.

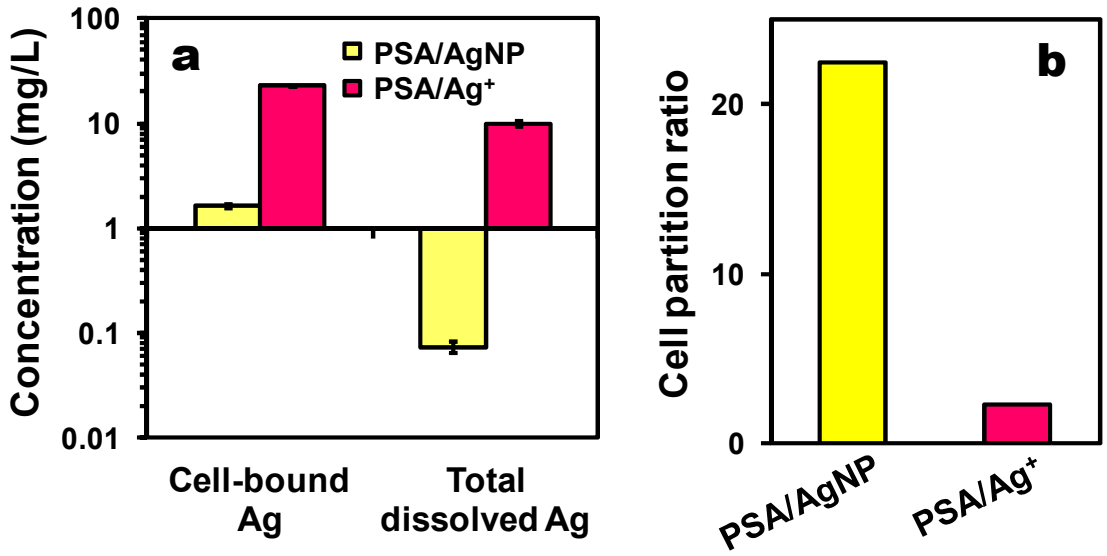

Fig. S14 Comparison of (a) the cell-bound and total dissolved Ag concentrations, and (b) cell partition ratios of *E. coli* cells exposed to PSA/AgNP and PSA/Ag^+ cryogels. Note that the cell partition ratio was computed by taking the ratio of the cell-bound Ag concentration to that of the dissolved Ag.

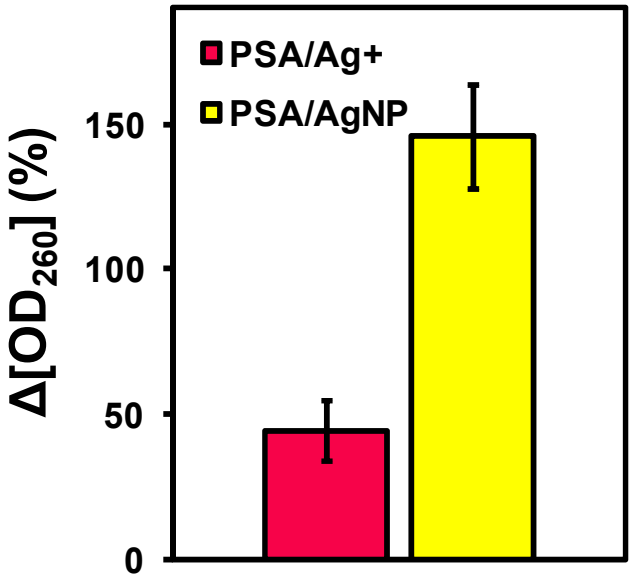

Fig. S15 Degree of cytoplasmic content release by *E. coli* cells contacted with PSA/Ag^+ or PSA/AgNP cryogels. Note that a higher OD_{260} indicates the release of more cytoplasmic contents.

References

(1) Cordelires, F.; Jackson, J., 3D object counter. In http://rsb.info.nih.gov/ij/plugins/track/objects.html (accessed 27/02/2014).

(2) Doube, M.; Kłosowski, M. M.; Arganda-Carreras, I.; Cordelières, F. P.; Dougherty, R. P.; Jackson, J. S.; Schmid, B.; Hutchinson, J. R.; Shefelbine, S. J., BoneJ: Free and extensible bone image analysis in ImageJ. *Bone* **2010,** *47*, (6), 1076-1079.

(3) Darling, A. L.; Sun, W., 3D microtomographic characterization of precision extruded poly-e-caprolactone scaffolds. *Journal of Biomedical Materials Research Part B: Applied Biomaterials* **2004,** *70B* 311-17.

(4) Lin, A. S. P.; Barrows, T. H.; Cartmell, S. H.; Guldberg, R. E., Microarchitectural and mechanical characterization of oriented porous polymer scaffolds. *Biomaterials* **2003,** *24*, (3), 481-489.

(5) Savina, I. N.; Gun'ko, V. M.; Turov, V. V.; Dainiak, M.; Phillips, G. J.; Galaev, I. Y.; Mikhalovsky, S. V., Porous structure and water state in cross-linked polymer and protein cryo-hydrogels. *Soft Matter* **2011,** *7*, (9), 4276-4283.